

NSG 7052

A Three-Dimensional Viscoelastic Model of a Strike Slip Fault

Summary

An analytic approximation to the Green's function for the displacements due to a strike slip point source in an elastic layer over a viscoelastic half-space is developed. This approximate Green's function is useful because it can be analytically integrated over the fault surface. Comparison with a numerical integration of the exact solution integral indicates that the approximation is quite good. The approximate Green's function is integrated analytically to obtain the displacements due to a finite rectangular strike slip fault in an elastic layer over a viscoelastic half-space. Ground displacements and angle changes from a model survey net are computed to illustrate the viscoelastic relaxation which follows a fracture in the elastic region.

(NASA-CR-148584) A THREE-DIMENSIONAL N76-29785
VISCOELASTIC MODEL OF A STRIKE SLIP FAULT
(California Univ.) 51 p HC \$4.50 = CSCL 08E
Unclas
G3/46 49530 -



Recently there has been a growing interest in the use of static or quasistatic displacements, strains and tilts for the investigation of earthquake-related phenomena. In particular, aseismic horizontal surface displacements due to the San Andreas fault have been studied extensively (Savage & Burford 1973; Thatcher 1974, 1975a,b) by the use of geodetic triangulation techniques. The importance of the San Andreas lies in its well-documented history (Meade 1973) of aseismic surface motions. With this data we can learn much about the processes involved in pre and postseismic displacements and in tectonic plate motion.

Observations of surface movements due to the San Andreas can be interpreted by means of mathematical models obtained by idealizing the fault as a vertical fracture in an elastic medium. The models describing near field displacements are obtained by integration of a Green's function for a strike slip source. For convenience, the source is usually assumed to be located in an elastic half-space whose elastic properties may vary with depth. Although the Green's function has been computed for both line and point sources in layered half-spaces (Ben-Menahem & Singh 1968; Rybicki 1971; Chinnery & Jovannovich 1972; Jovannovich et al. 1974a,b) the Green's function for a point source has not been analytically integrated over a fault surface. The line source Green's function is really only useful in describing a fault whose dislocation function changes slowly along its strike. The point source Green's function can be used to describe a finite-dimensional fault with an arbitrary dislocation function.

In this paper we construct a model for a rectangular vertical strike slip fault which can be used to explain the post-seismic surface displacements occurring after a large earthquake. We propose to represent the fault as a fracture in an elastic layer over a viscoelastic half-space, a model conceptually similar to that proposed by Nur and Mavko (1974) for infinitely long, dipping thrust faults. Unlike the Nur-Mavko model however, ours describes a vertical, finite-dimensional strike slip fault. In both models, the displacements from a fracture in an elastic layer overlying an elastic half-space are first computed, and the correspondence principle (Biot 1954; Lee 1955; Fung 1965) is then used to introduce Newtonian viscoelastic properties into the half-space.

We base our model on an approximate representation of the Green's function for horizontal displacements due to a strike slip point source in an elastic layer over an elastic half-space. Although the exact expression for the Green's function has been found (Ben-Menahem & Singh 1968), it is in the form of an integral over a Fourier wave number k . In our model, three additional integrations of this Green's function are needed: two over the fault surface and an inverse Laplace transform from use of the correspondence principle. These four integrals can be done numerically, but since near field displacements are desired over a wide range of times, small mesh sizes are needed in the integrations. The approximate Green's function described below is accurate, easy to use and has the advantage that all the succeeding integrations can be done analytically. Thus the

inverse problem (Rundle & Jackson 1976a,b) can be done simply using analytically computed partial derivatives.

An Approximate Image Technique

Ishii and Takagi (1967) solved a two-dimensional problem for the displacements from a line force located at the coordinates $x_3, x_2 = 0$, in an infinite elastic medium whose rigidity changes abruptly at $y_3 = 0$ (figure 1). Rybicki (1971) showed that the equations of elasticity for this case reduce to Poisson's equation. He was thus able to use the method of images (figure 2) to find the displacements from a line source in and below a horizontal layer over a half-space. For an infinite medium whose $y_1 - y_2$ plane divides the space into two parts, one of rigidity μ_1 and another of rigidity μ_2 , we can write the displacements in the y_1 -direction at a point (y_2, y_3) due to a line force at (x_2, x_3) of unit magnitude:

$$-\frac{1}{2\pi\mu_1} \left[\log\sqrt{(y_2 - x_2)^2 + (y_3 - x_3)^2} + \frac{\mu_1 - \mu_2}{\mu_1 + \mu_2} \log\sqrt{(y_2 - x_2)^2 + (y_3 + x_3)^2} \right]$$

for $y_3 \geq 0, x_3 \geq 0$

$$-\frac{1}{\pi(\mu_1 + \mu_2)} \log\sqrt{(y_2 - x_2)^2 + (y_3 - x_3)^2}$$

for $y_3 \geq 0, x_3 \leq 0$ and $y_3 \leq 0, x_3 \geq 0$

$K_1^1(y, x) = \{$

$$,, -\frac{1}{2\pi\mu_2} \left[\log\sqrt{(y_2 - x_2)^2 + (y_3 - x_3)^2} + \frac{\mu_2 - \mu_1}{\mu_2 + \mu_1} \log\sqrt{(y_2 - x_2)^2 + (y_3 + x_3)^2} \right]$$

for $y_3 \leq 0, x_3 \leq 0$

(1).

where μ_1 is the rigidity for $y_3 < 0$ and μ_2 is the rigidity for $y_3 > 0$. The superscript of κ_1^1 indicates the coordinate along which the displacement appears, and the subscript indicates the direction along which the force acts. The tilde under the variable denotes a vector.

It has been shown (Rybicki 1971) that the displacements V_{12}^1 at (x_2, x_3) due to an elementary single-couple line dislocation $U_0 dS$ at (y_2, y_3) across a vertical plane can be obtained from $k_1^1(\underline{y}, \underline{x})$ by the operation

$$V_{12}^1(\underline{x}, \underline{y}) = U_0 dS \mu \frac{\partial}{\partial y_2} \kappa_1^1(\underline{y}, \underline{x})$$

$$\mu \equiv \begin{cases} \mu_1 & y_3 < 0 \\ \mu_2 & y_3 > 0 \end{cases} \quad (2)$$

where U_0 is the magnitude of the dislocation and dS is the area over which it occurs. It is important to notice that the displacements $V_{12}^k(\underline{x}, \underline{y})$ at \underline{y} in direction k due to a strike slip source at \underline{y} are proportional to the horizontal (12) shear stresses at \underline{y} due to a unit force at \underline{x} in direction k .

We would like to find the displacements due to a line dislocation in a layered half-space. Using the coordinate system of figure 2, one can superpose image line forces to satisfy the requirements of a traction-free surface at $y_3 = 0$ and continuity of the solution and its consequent stresses at $y_3 = H$. The displacements from a line force in a layered half-space whose layer thickness is H (Rybicki 1971) is:

$$\begin{aligned}
G_1^1(x, x) &= -\frac{1}{2\pi\mu_1} \{ \log\sqrt{(y_2 - x_2)^2 + (y_3 - x_3)^2} + \log\sqrt{(y_2 - x_2)^2 + (y_3 + x_3)^2} \\
&\quad + \sum_{m=1}^{\infty} \left(\frac{\mu_1 - \mu_2}{\mu_1 + \mu_2} \right)^m \left[\log\sqrt{(y_2 - x_2)^2 + (y_3 - 2mH - x_3)^2} + \log\sqrt{(y_2 - x_2)^2 + (y_3 - 2mH + x_3)^2} \right. \\
&\quad \left. + \log\sqrt{(y_2 - x_2)^2 + (y_3 + 2mH - x_3)^2} + \log\sqrt{(y_2 - x_2)^2 + (y_3 + 2mH + x_3)^2} \right] \} \text{ for } y_3 \leq H, x_3 \leq H
\end{aligned}$$

$$\begin{aligned}
G_1^1(x, x) &= -\frac{1}{\pi(\mu_1 + \mu_2)} \{ \log\sqrt{(y_2 - x_2)^2 + (y_3 - x_3)^2} + \log\sqrt{(y_2 - x_2)^2 + (y_3 + x_3)^2} \\
&\quad + \sum_{m=1}^{\infty} \left(\frac{\mu_1 - \mu_2}{\mu_1 + \mu_2} \right)^m \left[\log\sqrt{(y_2 - x_2)^2 + (y_3 - 2mH - x_3)^2} + \log\sqrt{(y_2 - x_2)^2 + (y_3 + 2mH + x_3)^2} \right] \} \\
&\quad \text{for } y_3 \leq H, x_3 \geq H
\end{aligned}$$

$$\begin{aligned}
G_1^1(x, x) &= -\frac{1}{2\pi} \left\{ \frac{1}{\mu_2} \log\sqrt{(y_2 - x_2)^2 + (y_3 - x_3)^2} + \frac{1}{\mu_2} \frac{\mu_2 - \mu_1}{\mu_2 + \mu_1} \cdot \log\sqrt{(y_2 - x_2)^2 + (y_3 - 2mH + x_3)^2} \right. \\
&\quad + \frac{4\mu_1}{(\mu_1 + \mu_2)^2} \log\sqrt{(y_2 - x_2)^2 + (y_3 + x_3)^2} + \frac{4\mu_1}{(\mu_1 + \mu_2)^2} \sum_{m=1}^{\infty} \left(\frac{\mu_1 - \mu_2}{\mu_1 + \mu_2} \right)^m \\
&\quad \left. \cdot \log\sqrt{(y_2 - x_2)^2 + (y_3 + 2mH + x_3)^2} \right\} \text{ for } y_3 \geq H, x_3 \geq H \tag{3}
\end{aligned}$$

where μ_1 is the layer rigidity and μ_2 is the half-space rigidity. The operator $U_0 dS \mu \frac{\partial}{\partial y_2}$ can again be used to obtain the displacements at (x_2, x_3) due to a line strike slip source at (y_2, y_3) . Chinnery and Jovannovich (1972) have extended (3) to a many-layered half-space.

Equation (3) satisfies the conditions which uniquely define the Green's function for the linear differential operator, the Navier equation of elastostatic equilibrium, and the boundary conditions of the problem (Courant & Hilbert 1953, p. 353):

(i) For fixed x_2 and x_3 , $G_1^1(y, x)$ has a singularity in the stress at $y_2 = x_2$, $y_3 = x_3$. Thus in two dimensions $G_1^1(y, x)$ is proportional to the logarithm of the distance between observation and source points.

(ii) The displacements $G_1^1(y, x)$ and tractions on any horizontal plane are everywhere continuous except at $y_2 = x_2$, $y_3 = x_3$.

(iii) $G_1^1(y, x)$ satisfies the boundary conditions.

These three requirements imply that for the Green's function considered here, the reciprocal theorem holds: $G_1^1(y, x) = G_1^1(x, y)$.

Since we are interested in calculating displacements due to a finite-dimensional strike slip fault in an elastic layer over a viscoelastic half-space we must find the Green's function for a strike slip point source. Let us consider the situation in which a double-couple source at y_3 is in the layer and attempt to write down an approximate Green's function. The approximation must satisfy conditions (i) - (iii) as well as possible. For example, one can show that condition (ii) can be satisfied

using any function whose y_3 and x_3 arguments appear only in the form $(y_3 - x_3)^2$, $(y_3 + x_3)^2$, $(y_3 \pm 2mH \pm x_3)^2$, with the function occurring in the same term-by-term arrangement as the logarithms in equation (3). This suggests that we can apply the form of (3) to our three-dimensional problem.

We already know the exact analytic solution for the displacements $u_{12}^1(x, y)$ from a double-couple force in an infinite medium (Steketee 1958):

$$\begin{aligned}
 u_{12}^1(x, y) &= \frac{U_0 dS}{8\pi} \left[2(1 - \alpha) \frac{x_2}{R^3} + 6\alpha \frac{x_1^2 x_2}{R^5} \right] \\
 u_{12}^2(x, y) &= \frac{U_0 dS}{8\pi} \left[2(1 - \alpha) \frac{x_1}{R^3} + 6\alpha \frac{x_1 x_2^2}{R^5} \right] \\
 u_{12}^3(x, y) &= \frac{U_0 dS}{8\pi} \left[6\alpha \frac{x_1 x_2 (x_3 - y_3)}{R^5} \right].
 \end{aligned} \tag{4}$$

The double-couple source is located at $(0, 0, y_3)$ and the observation point is at x . $U_0 dS$ is the elementary displacement dislocation corresponding to the double-couple force, $\alpha = \frac{\lambda + \mu}{\lambda + 2\mu}$, and $R = \sqrt{x_1^2 + x_2^2 + (x_3 - y_3)^2}$. Again the superscript indicates the displacement direction, and the subscripts correspond to the fact that the u_{12}^k are derived by finding the horizontal shear stresses at y due to a point force at x , along coordinate k . Using the fact that equation (3) represents horizontal displacements due to horizontal forces, we can try the following

as an approximate Green's function:

$$\begin{aligned}
 W_{12}^1(x, y) &= \frac{U_0 ds}{8\pi} \left\{ 2(1-\alpha) \frac{x_2}{R^3} + \frac{6\alpha x_1^2 x_2}{R^5} + 2(1-\alpha) \frac{x_2}{S^3} + \frac{6\alpha x_1^2 x_2}{S^5} \right. \\
 &+ \sum_{m=1}^{\infty} \left(\frac{\mu_1 - \mu_2}{\mu_1 + \mu_2} \right)^m \left[2(1-\alpha) \frac{x_2}{R_{--}^3} + \frac{6\alpha x_1^2 x_2}{R_{--}^5} + \frac{2(1-\alpha) x_2}{R_{-+}^3} + \frac{6\alpha x_1^2 x_2}{R_{-+}^5} \right. \\
 &\left. \left. + \frac{2(1-\alpha) x_2}{R_{+-}^3} + \frac{6\alpha x_1^2 x_2}{R_{+-}^5} + \frac{2(1-\alpha) x_2}{R_{++}^3} + \frac{6\alpha x_1^2 x_2}{R_{++}^5} \right] \right\}
 \end{aligned}$$

for $x_3 \leq H, y_3 \leq H$

$$\begin{aligned}
 &\frac{2\mu_1}{\mu_1 + \mu_2} \left(\frac{U_0 ds}{8\pi} \right) \left\{ \frac{2(1-\alpha) x_2}{R^3} + \frac{6\alpha x_1^2 x_2}{R^5} + \frac{2(1-\alpha) x_2}{S^3} + \frac{6\alpha x_1^2 x_2}{S^5} \right. \\
 &\left. + \sum_{m=1}^{\infty} \left(\frac{\mu_1 - \mu_2}{\mu_1 + \mu_2} \right)^m \left[\frac{2(1-\alpha) x_2}{R_{--}^3} + \frac{6\alpha x_1^2 x_2}{R_{--}^5} + \frac{2(1-\alpha) x_2}{R_{++}^3} + \frac{6\alpha x_1^2 x_2}{R_{++}^5} \right] \right\}
 \end{aligned}$$

for $x_3 \leq H, y_3 \geq H$ (5)

where

$$S^2 = x_1^2 + x_2^2 + (x_3 + y_3)^2; \quad \alpha = \frac{\lambda + \mu_1}{\lambda + 2\mu_1}$$

$$R_{++}^2 = x_1^2 + x_2^2 + (x_3 + 2mH + y_3)^2$$

$$R_{+-}^2 = x_1^2 + x_2^2 + (x_3 + 2mH - y_3)^2$$

$$R_{-+}^2 = x_1^2 + x_2^2 + (x_3 - 2mH + y_3)^2$$

$$R_{--}^2 = x_1^2 + x_2^2 + (x_3 - 2mH - y_3)^2$$

where again μ_1 is the layer rigidity and μ_2 is the half-space rigidity.

This trial Green's function has a singularity at the proper point; its contribution to displacement is continuous at $x_3 = H$; and its contribution to shearing stress, $\mu \frac{\partial w_{12}^1}{\partial x_1}$, and normal stress, $\lambda \frac{\partial w_{12}^1}{\partial x_3}$ is continuous at $x_3 = H$ if $\lambda_1 = \lambda_2$, which we shall henceforth assume. However, it is evident that there still exists a normal stress at $x_3 = 0$, and thus the surface is not stress-free. We can remedy this defect by adding to each source and its image a term corresponding to the displacements that result from superposing a normal stress to cancel the normal stress mentioned above:

$$g_{12}^1(x, y) = \frac{U_0 ds}{8\pi} \left\{ \frac{x_2}{r^4} \left(A + \frac{x_1^2}{r^2} B \right) + \sum_{m=1}^{\infty} \left(\frac{\mu_1 - \mu_2}{\mu_1 + \mu_2} \right)^m \frac{x_2}{r^4} \left(A_+ + \frac{x_1^2}{r^2} B_+ \right) + \frac{x_2}{r^4} \left(A_- + \frac{x_1^2}{r^2} B_- \right) \right\}$$

$$\text{for } x_3 = 0, \text{ source at } (0, 0, y_3), y_3 \leq H \quad (6)$$

$$g_{12}^1(x, y) = \frac{2\mu_2}{\mu_1 + \mu_2} \frac{U_0 ds}{8\pi} \left\{ \frac{x_2}{r^4} \left(A + \frac{x_1^2}{r^2} B \right) + \sum_{m=1}^{\infty} \left(\frac{\mu_1 - \mu_2}{\mu_1 + \mu_2} \right)^m \frac{x_2}{r^4} \left(A_+ + \frac{x_1^2}{r^2} B_+ \right) \right\}$$

$$\text{for } x_3 = 0, \text{ source at } (0, 0, y_3), y_3 \geq H$$

where

$$A = -4y_3 + 2\rho + 2\frac{y_3}{\rho}; \quad \rho^2 = x_1^2 + x_2^2 + y_3^2$$

$$B = 16y_3 + 6\rho - 48\frac{y_3^2}{\rho} + 38\frac{y_3^4}{\rho^3} - 12\frac{y_3^6}{\rho^5}$$

$$A_+ = -4(y_3 + 2mH) + 2\rho_+ + 2\frac{(y_3 + 2mH)^2}{\rho_+};$$

$$\rho_+ = x_1^2 + x_2^2 + (y_3 + 2mH)^2$$

$$B_+ = 16(2mH + y_3) + 6\rho_+ - 48 \frac{(2mH + y_3)^2}{\rho_+} + 38 \frac{(y_3 + 2mH)^4}{\rho_+^3} - 12 \frac{(y_3 + 2mH)^6}{\rho_+^5}$$

$$A_- = -4(2mH - y_3) + 6\rho_- + 2 \frac{(2mH - y_3)^2}{\rho_-};$$

$$\rho_- = x_1^2 + x_2^2 + (2mH - y_3)^2$$

$$B_- = 16(2mH - y_3) + 6\rho_- - 48 \frac{(2mH - y_3)^2}{\rho_-} + 38 \frac{(2mH - y_3)^4}{\rho_-^3} - 12 \frac{(2mH - y_3)^6}{\rho_-^5}$$

$$r^2 = x_1^2 + x_2^2$$

Note that each term of the form $\frac{U_0 dS}{8\pi} \frac{x_2}{r^4} (A_{\pm} + \frac{x_1^2}{r^2} B_{\pm})$ is the Green's function for a strike slip point source at depth $2mH \pm y_3$ in a homogeneous half-space for observation points at the free surface $x_3 = 0$ (Steketee 1958). Thus for observation points $x_3 > 0$, $g_{12}^1(x, y)$ can be written out by substituting for each Green's function for $x_3 = 0$ the corresponding Green's function for arbitrary x_3 as found by Steketee (1958).

The surface $x_3 = 0$ is now stress-free, but $g_{12}^1(x, y)$ and its associated contribution to the stresses are no longer continuous at $x_3 = H$. We are missing a set of terms which "fixes up" $g_{12}^1(x, y)$ and makes it smoothly continuous across the boundary between layer and half-space. Since we are limited to

the observation of surface motion however, it is necessary only to insure that this approximate solution is nearly equal to the real solution for observation points at $x_3 = 0$.

We shall postpone further discussion of the accuracy of the approximate Green's function to a later section. Instead we complete the development of the model by integrating (6) over a rectangular fault surface and introducing viscoelastic properties into the half-space.

The Finite Fault

The solution for horizontal displacements due to a finite fault can be found by integrating (6) over the area of the fault according to the well-known Volterra relation (Steketee 1958):

$$u_m^k(\underline{y}) = \iint_{\text{fault surface}} \Delta u_i(\underline{x}) g_{i\epsilon}^k(\underline{x}, \underline{y}) n_\epsilon dS(\underline{x}) \quad (7)$$

where n_ϵ is the outward normal to the fault surface and Δu_i is the displacement jump. Both a lower tilde and index notation are used to denote vectors and the summation convention is assumed. An upper carat denotes a unit vector.

Note that the observation point is now located at \underline{y} , and the integral is performed over the variable \underline{x} . Performing (7) over a rectangular strike slip fault of semilength L with top at depth d , bottom at depth D and with $\Delta u_i = U \hat{x}_i = \text{constant}$ is particularly easy. The result can be taken from the literature (Chinnery 1961, 1963) using the coordinate system of figure 3. For $y_3 = 0$, $x_3 \leq H$, the case of interest here,

$$\begin{aligned}
u_1 = & \frac{U_0}{4\pi} \left\{ y_2 t \alpha \left(\frac{1}{s_1 (s_1 + q)} + \frac{(1+c)s_2 + (1-b)p + q}{s_2 (s_2 + p)^2} - \frac{(p^2 - q^2)(2s_2 + p)}{2s_2^3 (s_2 + p)^2} \right) \right. \\
& + \tan^{-1} \frac{qt}{y_2 s_1} + \tan^{-1} \frac{pt}{y_2 s_2} + \sum_{m=1}^{\infty} \left(\frac{\mu_1 - \mu_2}{\mu_1 + \mu_2} \right)^m y_2 t \alpha \left(\frac{1}{s_{1+} (s_{1+} + q_+)} + \frac{(1+c)s_{2+} + (1-b)p_+ + q_+}{s_{2+} (s_{2+} + p_+)^2} \right. \\
& \left. - \frac{(p_+^2 - q_+^2)(2s_{2+} + p_+)}{2s_{2+}^3 (s_{2+} + p_+)^2} \right) + \tan^{-1} \frac{q_+ t}{y_2 s_{1+}} + \tan^{-1} \frac{p_+ t}{y_2 s_{2+}} + y_2 t \alpha \left(\frac{1}{s_{1-} (s_{1-} + q_-)} \right. \\
& \left. + \frac{(1+c)s_{2-} + (1-b)p_- + q_-}{s_{2-} (s_{2-} + p_-)^2} - \frac{(p_-^2 - q_-^2)(2s_{2-} + p_-)}{2s_{2-}^3 (s_{2-} + p_-)^2} \right) + \tan^{-1} \frac{q_- t}{y_2 s_{1-}} + \tan^{-1} \frac{p_- t}{y_2 s_{2-}} \left. \right\} \quad (8)
\end{aligned}$$

$$\begin{aligned}
u_2 = & \frac{U_0}{4\pi} \left\{ (1-\alpha) \ln(s_1 + q) + (1-\alpha-\alpha c) \ln(s_2 + p) - \alpha \left(\frac{(b+c)p - q}{s_2 + p} + \frac{(p^2 - q^2)}{2s(s_2 + p)} \right) \right. \\
& - y_2^2 \alpha \left(\frac{1}{s_1 (s_1 + q)} + \frac{(1+c)s_2 + (1-b)p + q}{s_2 (s_2 + p)^2} - \frac{(p^2 - q^2)(2s_2 + p)}{2s_2^3 (s_2 + p)^2} \right) + \sum_{m=0}^{\infty} \left(\frac{\mu_1 - \mu_2}{\mu_1 + \mu_2} \right)^m \\
& \cdot \left[(1-\alpha) \ln(s_{1+} + q_+) + (1-\alpha-\alpha c) \ln(s_{2+} + p_+) - \alpha \left(\frac{(b+c)p_+ - q_+}{s_{2+} + p_+} + \frac{(p_+^2 - q_+^2)}{2s_{2+} (s_{2+} + p_+)} \right) \right. \\
& \left. - y_2^2 \alpha \left(\frac{1}{s_{1+} (s_{1+} + q_+)} + \frac{(1+c)s_{2+} + (1-b)p_+ + q_+}{s_{2+} (s_{2+} + p_+)^2} - \frac{(p_+^2 - q_+^2)(2s_{2+} + p_+)}{2s_{2+}^3 (s_{2+} + p_+)^2} \right) + (1-\alpha) \ln(s_{1-} + q_-) \right. \\
& \left. + (1-\alpha-\alpha c) \ln(s_{2-} + p_-) - \alpha \left(\frac{(b+c)p_- - q_-}{s_{2-} + p_-} + \frac{(p_-^2 - q_-^2)}{2s_{2-} (s_{2-} + p_-)} \right) - y_2^2 \alpha \left(\frac{1}{s_{1-} (s_{2-} + q_-)} \right) \right.
\end{aligned}$$

$$+ \frac{(1+c)s_{2-} + (1-b)p_{-} + q_{-}}{(s_{2-} + q_{-})^2} - \frac{(p_{-}^2 - q_{-}^2)(2s_{2-} + p_{-})}{2s_{2-}^3 (s_{2-} + p_{-})^2} \Big] \Big|$$

for $x_3 \leq H$, $\psi_3 = 0$

(9)

where

$$p = x_3 + y_3 \quad q = x_3 - y_3$$

$$p_+ = x_3 + y_3 + 2mH \quad q_+ = x_3 - y_3 - 2mH$$

$$p_- = x_3 - y_3 + 2mH \quad q_- = x_3 + y_3 - 2mH$$

$$t = x_1 - y_1 \quad a = \frac{\lambda_1 + \mu_1}{\lambda_1 + 2\mu_1}$$

$$b = \frac{\lambda_1 - \mu_1}{\lambda_1 + \mu_1}$$

$$c = \frac{\mu\lambda_1}{(\lambda_1 + \mu_1)^2}$$

$$s_1^2 = t^2 + y_2^2 + q^2 \quad s_2^2 = t^2 + y_2^2 + p^2$$

$$s_{1+}^2 = t^2 + y_2^2 + q_+^2 \quad s_{2+}^2 = t^2 + y_2^2 + p_+^2$$

$$s_{1-}^2 = t^2 + y_2^2 + q_-^2 \quad s_{2-}^2 = t^2 + y_2^2 + p_-^2$$

The notation $||$ is taken from Chinnery (1961, 1963) and has the meaning $f(x_1, x_3) || = f(+L, D) - f(+L, d) - f(-L, D) + f(-L, d)$.

Introduction of Time Dependence

Having found the displacements due to a finite-dimensional fault in an elastic layer of rigidity μ_1 over an elastic half-space of rigidity μ_2 , we modify the solution to add Newtonian viscous properties to the half-space. It is not our purpose here to enter the debate upon the rheological properties of the earth's constitutive material. We remark, however, that a Newtonian flow law may be justified for the shallow viscoelastic regions in the earth (McKenzie 1968) although there is evidence for nonlinear rheology as well (Post & Griggs 1973; Stocker & Ashby 1973). In addition, it has been shown that under some conditions a Newtonian rheology produces flow structures very similar to a rheology in which the strain rate depends upon the cube of the deviatoric stress (Parmentier et al. 1976). Thus we conclude that the use of a Newtonian flow rheology for our half-space is justified provided it is recognized that the viscosity may be an "average" in the sense of Parmentier et al. (1976).

It may also be that mineral rheology plays little role in the stress relaxation process. Since the zone of brittle fracture ends at a relatively shallow depth on the San Andreas (Brace & Byerlee 1970), an alternative source of the viscous properties of the lower viscoelastic zone may be transient flow of water in porous rock (e.g. Nur & Schultz 1973). Darcy's law, which governs hydrogeologic flow, implies that the stress relaxation process is essentially linear. Thus to a good

approximation, the half-space can be assumed to be a linear viscoelastic solid.

To add viscous properties to the half-space, we use the correspondence principle (Biot 1954; Lee 1955; Fung 1965) as outlined in the introduction. This principle states that if the elastic solution to a problem is known and the inertial forces are negligible, the quasistatic solution for a linear viscoelastic medium is obtained by replacing all time-dependent quantities by their Laplace transforms and then taking the inverse transform of the resulting expression. In the case of (6) or (8), we replace μ_2 by $\mu_2(s)$ and $U_0 H(t)$ by U_0/s , where $H(t)$ is the Heaviside step function, t is time and s is the conjugate Laplace variable.

We choose the properties of the half-space to be those of a Maxwell viscoelastic solid whose elastic constants are the same as those of the layer. This choice of Maxwell properties is motivated by the observation that for times short compared to a year the earth behaves elastically, while for longer times permanent non-elastic deformations are observed, for example in areas of crustal rebound (McConnell 1965; Crittenden 1968; Peltier, 1974) and in tectonically active fault zones during recent geologic history.

The Maxwell solid is the simplest kind of medium to exhibit this dual behavior. A Maxwell element is shown in figure 4; if a constant displacement is suddenly applied to the free end, the spring will immediately stretch. In the course of time, the spring will gradually unstretch as the piston in the dashpot

moves. The constitutive equation for a Maxwell solid is

$$\frac{\partial}{\partial t} \sigma_{ij} + \gamma \sigma_{kk} \delta_{ij} + \frac{2\mu_0}{\eta} \sigma_{ij} = \frac{\partial}{\partial t} (\lambda e_{kk} \delta_{ij} + 2\mu_0 e_{ij}) \quad (10)$$

where σ_{ij} is the stress tensor, e_{ij} is the strain tensor, δ_{ij} is the Kronecker delta, μ_0 is a constant rigidity and η is the viscosity. The constants λ and γ are related to compressional stresses which are assumed not to relax.

Upon performing the Laplace transform on (10), we can set

$$\mu_2(s) = \frac{\mu_0 s}{s + 2\mu_0/\eta} = \frac{\mu_0 s}{s + 2/\tau} \quad (11)$$

$$\mu_1(s) = \mu_0 \quad \tau = \eta/\mu_0$$

τ is a characteristic time constant for the system. Since the rigidity of the Maxwell medium has been chosen equal to that of the layer, only the effective viscosity η remains unknown.

After insertion of (11) in (8) and (9) we must find the inverse Laplace transform $L^{-1}[\]$ of quantities such as

$$\frac{1}{s} \left[\frac{\mu_0 s - \frac{\mu_0 s}{s + 2/\tau}}{\mu_0 s + \frac{\mu_0 s}{s + 2/\tau}} \right]^m = \frac{1}{\tau^m} \frac{1}{s} \left(\frac{1}{s + 1/\tau} \right)^m \quad (12)$$

From Abramowitz and Stegun (1970) we find

$$L^{-1} \left[\frac{1}{\tau^m} \frac{1}{s} \left(\frac{1}{s + 1/\tau} \right)^m \right] = H(t) \left(1 - e^{-t/\tau} \sum_{n=0}^{m-1} \left(\frac{t}{\tau} \right)^n \frac{1}{n!} \right) \quad (13)$$

Upon insertion of (13) into (8) and (9) we get expressions of the form

$$\begin{aligned} u_1(y) &= U_0 H(t) F_1(y) \left[1 + \sum_m \left\{ 1 - e^{-t/\tau} \sum_{n=0}^{m-1} \left(\frac{t}{\tau}\right)^n \frac{1}{n!} \right\} (A_{m+}(y) + A_{m-}(y)) \right] \\ u_2(y) &= U_0 H(t) F_2(y) \left[1 + \sum_m \left\{ 1 - e^{-t/\tau} \sum_{n=0}^{m-1} \left(\frac{t}{\tau}\right)^n \frac{1}{n!} \right\} (B_{m+}(y) + B_{m-}(y)) \right] \end{aligned} \quad (14)$$

where the $A_m(y)$ and $B_m(y)$ can be found from (8) and (9) and the $F_i(y)$ are the uniform elastic half-space solutions.

Upon examination of (14) it is clear that the first response of the system is entirely elastic. As time proceeds, successive terms under the summation on m become progressively more important. In the limit $t \rightarrow \infty$, the exponential dies away and we get

$$\begin{aligned} u_1(y) &= U_0 H(t) F_1(y) \left[1 + \sum_m (A_{m+}(y) + A_{m-}(y)) \right] \\ u_2(y) &= U_0 H(t) F_2(y) \left[1 + \sum_m (B_{m+}(y) + B_{m-}(y)) \right] \end{aligned} \quad (15)$$

Numerical tests indicate that only the first five terms need be retained under the sum in (14) for convergence accuracy within 1% for $t \leq 2\tau$. Since $A_{m\pm}(y)$ and $B_{m\pm}(y)$ have the same sign as $F_1(y)$ respectively $F_2(y)$, we arrive at the conclusion that with the viscoelastic model (14) the quasistatic stress relaxation tends to increase the displacements found immediately after the fracture.

For a long fault which breaks entirely through the elastic

layer, the post-fracture viscoelastic displacements can be an appreciable fraction of the initial movement (figures 5 - 9). Within ten kilometers of the fault shown, there is a relatively small amount of post-fracture movement compared to the rupture-induced displacements. Between approximately ten and one hundred kilometers, the post-fracture displacements diminish slowly with distance at any given time. At distances of more than thirty kilometers from the fault, most of the total movement is accounted for by viscoelastic effects rather than by the initial elastic response. We thus obtain surface strains increasingly concentrated near the rupture as time progresses.

Observations of strains localized near the San Andreas fault following 1906 led Thatcher (1975a) to postulate his aseismic sliding model, but as shown here it is also true that such a strain distribution can equally well be explained by anelastic adjustment. The important point is that whereas stable sliding tends to alleviate overall strain buildup and thus increase the time interval between shocks, viscoelastic adjustment has the opposite effect of increasing the stress on the fault following the earthquake and thus decreasing the waiting time until the next shock.

As another illustration, angle changes for the model triangulation networks in figure 10 have been computed from equations (8), (9) and (14) and the results are shown in Table 1. The most important factor determining transient motion due to viscoelastic adjustment within each time interval $\Delta t = \tau = \eta/\mu_0$ is the relationship of the elastic layer thickness H to the

fault plane height $D - d$. If $H \sim D - d$, the amount of post-rupture movement will be large; if $H \gg D - d$, the motion will be small.

Accuracy of the Green's Function

To determine the accuracy of g_{12}^1 , we can compare the surface displacements computed from the approximate Green's function, equation (6), with those obtained from a numerical integration of the exact solution (Ben-Menahem & Singh 1968). Note the error in equation (11-57) of Ben-Menahem and Singh (1968), which is corrected in Jovannovich et al. (1974a). The integration was performed using the IBM-supplied Scientific Subroutine Package.

In presenting the results of the surface displacement calculations we adopt the Jovannovich et al. (1974b) convention of $U_0 = 1$ km and $dS = 1$ km². The worst agreement between equation (6) and the exact solution is expected when the source point is near the layer/half-space boundary, because the displacements and stresses implicit in the approximate Green's function are not continuous there. Tables 2 - 3 and figures 11 - 12 are examples of comparisons between exact and approximate Green's functions.

In figure 11 and table 2, the layer thickness has been chosen equal to 10 km. Using fault parameters appropriate to the San Andreas as in Rundle and Jackson (1976b), use was made of Thatcher's (1974b) result that the fracture of the 1906 San Francisco earthquake extended to a depth of 10 km. The elastic layer was therefore constrained to be at least 10 km thick. Since the fault plane extends from the surface to 10 km depth, it is natural to check the approximate Green's function for $H = 10$ km, since as stated above, the approximation is expected

to be worst for this case.

In figure 11 and table 2, the source depth is varied from 10 to 1 km in 1 km increments. The point of observation was located at a radial distance of 10 km from the epicenter of the source. The error is defined as $\{(\text{approximate surface displacement} - \text{exact surface displacement}) / (\text{approximate surface displacement})\} \times 100\%$. It is evident that the greatest errors in the approximate Green's function occur when the source is near the layer/half-space boundary. Above and below a source depth of about 5 km the difference between exact and approximate Green's functions has opposite sign. Upon integrating the Green's function over the entire 10 km depth, the errors tend to compensate in this case.

To estimate the error in the displacements from a finite, rectangular fault obtained using equation (6), we can sum the entries in column 2 of table 2 and divide them by the sum of the entries in column 3. The result of this calculation indicates that the discrepancy in the displacements caused by using (8), (9) and (14) in place of the exact solution is small.

Figure 12 and table 3 illustrate the effect of a changing elastic layer thickness H upon the surface displacements due to a source fixed at 10 km depth. The point of observation was again located at an epicentral distance of 10 km, while H was varied from 10 to 30 km in 5 km increments. As shown, the error in the surface displacements decreases sharply as the interface is removed to a greater depth. For thicknesses H greater than 15 km, the error is never greater than 5% in

magnitude.

Note that equation (6) is essentially a perturbation expansion in the quantity $\frac{\mu_1 - \mu_2}{\mu_1 + \mu_2} \equiv \xi$ about the homogeneous half-space Green's function for $y_3 \leq H$, $x_3 \leq H$, and is a similar expansion multiplied by the constant $2\mu_2/(\mu_1 + \mu_2)$ for $x_3 \leq H$, $y_3 \geq H$. From the observation that successive terms represent more deeply buried "sources" of the same strength, thus giving rise to smaller contributions to the surface displacements, we can write the series in the form

$$g_{12}^1(x, y) = F_1(x, y) \left\{ 1 + \sum_{m=1}^{\infty} \xi^m \left[A_m(x, y) + B_m(x, y) \right] \right\} \quad y_3 \leq H, x_3 \leq H \quad (16)$$

$$g_{12}^1 = \frac{2\mu_2}{\mu_1 + \mu_2} F_1(x, y) \left\{ 1 + \sum_{m=1}^{\infty} \xi^m \left[A_m(x, y) \right] \right\} \quad y_3 \geq H, x_3 \leq H$$

where $F_1(x, y)$ is the Green's function for a source in a homogeneous half-space, and A_m and B_m are defined as in (6). Note that $A_m(x, y)$ and $B_m(x, y)$ are positive definite since they are derived from terms under the summation in (6) which all have the same sign as $F_1(x, y)$. $A_m(x, y)$ and $B_m(x, y)$ are also bounded, and because $|\xi| < 1$ for all physical earth models, both series in (16) converge (e.g., Whittaker & Watson 1927, p. 11).

We can show that the representation (6) has the correct limiting properties. For the case $\mu_1 = \mu_2$, g_{12}^1 and g_{12}^2 reduce to the Green's function for the homogeneous half-space. Also, we know that integration of the solution for a point source along a line gives rise to the solution for a line source, so integration of the infinite series of point sources represented by (6) along a line parallel to the x_1 axis yields Rybicki's

(1971) Green's function. Finally, as we let H go to infinity in the upper of (6), the terms under the summation vanish, whereas if H approaches zero in the lower of (6) we get

$$\begin{aligned} \lim_{H \rightarrow 0} g_{12}^1(x, y) &= \frac{2\mu_2}{\mu_1 + \mu_2} F_1(x, y) \left\{ 1 + \sum_{m=1}^{\infty} \left(\frac{\mu_1 - \mu_2}{\mu_1 + \mu_2} \right)^m \right\} \\ &= \frac{2\mu_2}{\mu_1 + \mu_2} F_1(x, y) \frac{1}{1 - \frac{\mu_1 - \mu_2}{\mu_1 + \mu_2}} = F_1(x, y) \end{aligned} \quad (17)$$

The fact that the solution to this problem can be represented fairly accurately as a rapidly converging series in the parameter ξ suggests a method for the evaluation of exact integral solutions for problems of this type. At present, the integration of the exact Green's function has been done numerically by approximating the denominator as a finite series of exponentials (Ben-Menahem & Gillon 1970). Upon examination of the exact Green's function integral, equation 11-56 of Ben-Menahem and Singh (1968), we see that if we write

$$\begin{aligned} \xi &= \frac{1 - \nu}{1 + \nu} & \mu_{HS} &= \nu \mu_L \\ \nu &= \frac{1 - \xi}{1 + \xi} & \delta_{HS} &= \frac{\lambda + \mu_L \nu}{\lambda + 2\mu_L} = \frac{\lambda + \mu_L \left(\frac{1 - \xi}{1 + \xi} \right)}{\lambda + 3\mu_L \left(\frac{1 - \xi}{1 + \xi} \right)} \end{aligned} \quad (18)$$

we can expand the integrand in powers of ξ . The convergence properties of the series can be investigated and if (6) is an indication, term-by-term integration can probably be carried out. The advantage of this procedure is that it may well put the integral in a form which is more amenable to analytic solution.

We know in advance that the first term must be the Green's function for the homogeneous half-space and thus we know its algebraic representation (Steketee, 1958). In addition, the modelling of an elastic layer over a viscoelastic half-space via the correspondence principle is particularly easy due to the isolation of the elastic constants in the factor ξ . One can extend this procedure to half-spaces of many layers by using multiple sums of several parameters $\xi_i = \frac{\mu_i}{\mu_0}$ where μ_0 is the rigidity of a particular reference layer.

Summary

We constructed an accurate analytic approximation to the Green's function for a vertical strike-slip fault in an elastic layer over an elastic half-space. To model the San Andreas fault, we integrated the Green's function over a rectangular surface and introduced linear viscoelasticity into the half-space by means of the correspondence principle. Examples of viscoelastic relaxation in the form of post-fracture surface displacements and angle changes from a model triangulation net were computed.

J.B. Rundle and D.D. Jackson

Department of Geophysics and Space Physics

University of California

Los Angeles, California 90024

Acknowledgements

This research was supported by NASA grant NSG-7002.

References

- Abramowitz, M. & Stegun, I., Eds., 1970. Handbook of Mathematical Functions with Formulas, Graphs, and Mathematical Tables, U.S.G.P.O., Washington, D.C.
- Ben-Menahem, A. & Gillon, A., 1970. Crustal deformation by earthquakes and explosions, Bull. seism. Soc. Am., 60, 193.
- Ben-Menahem, A. & Singh, S., 1968. Multipolar elastic fields in a layered half-space, Bull. seism. Soc. Am., 58, 1519.
- Biot, M., 1954. Theory of stress-strain relation in anisotropic viscoelasticity and relaxation phenomena, J. appl. Phys., 25, 1385.
- Brace, W. & Byerlee, J., 1970. California earthquakes: Why only shallow focus?, Science, 168, 1573.
- Chinnery, M., 1961. The deformation of the ground around surface faults, Bull. seism. Soc. Am., 51, 355.
- Chinnery, M., 1963. The stress changes that accompany strike-slip faulting, Bull. seism. Soc. Am., 53, 921.
- Chinnery, M. & Jovannovich, D., 1972. Effect of earth layering on earthquake displacement fields, Bull. seism. Soc. Am., 62, 1629.
- Courant, R. & Hilbert, D., 1953. Methods of Mathematical Physics, Interscience, New York.
- Crittenden, M., 1963. Effective viscosity of the earth derived from isostatic loading of Pleistocene Lake Bonneville, J. Geophys. Res., 68, 5517.

- Fung, Y., 1965. Foundations of Solid Mechanics, Prentice-Hall, Englewood Cliffs, New Jersey.
- Ishii, H. & Takagi, A., 1967. Theoretical study on the crustal movements Part II: The influence of horizontal discontinuity, Tôkhoko Daigaku Sci. Reports Geophys., ser. 5, 19, 95.
- Jovannovich, D., Hussein M. & Chinnery, M., 1974a. Elastic dislocations in a layered half-space--I: Basic theory and numerical methods, Geophys. J. R. astr. Soc., 39, 205.
- Jovannovich, D., Hussein, M. & Chinnery, M., 1974b. Elastic dislocations in a layered half-space--II: The point source, Geophys. J. R. astr. Soc., 39, 219.
- Lee, E., 1955. Stress analysis in visco-elastic bodies, Quart. J. appl. Math., 13, 183.
- McConnell, R., 1965. Isostatic adjustment in a layered earth, J. geophys. Res., 70, 5171.
- McKenzie, D., 1968. The geophysical importance of high temperature creep, in The History of the Earth's Crust, Phinney, R., Ed., Princeton Univ. Press.
- Meade, B., Ed., 1973. Reports on Geodetic Measurements of Crustal Movement, 1906-71, U.S.G.P.O. Publ. No. 0317-00167, Rockville, Maryland.
- Nur, A. & Mavko, G., 1974. Postseismic viscoelastic rebound, Science, 183, 204.
- Nur, A. & Schultz, P., 1973. Fluid flow and faulting, 2: A stiffness model for seismicity, Proc. Conf. Tectonic Problems San Andreas Fault System, Nur, A. & Kovach, R., Eds., Stanford

Univ. Publ. Geol. Sci., 14.

- Parmentier, E., Turcotte, D. & Torrance, K., 1976. Studies of finite amplitude non-Newtonian thermal convection with application to convection in the earth's mantle, J. geophys. Res., 81, 1839.
- Peltier, W.R., 1974. The impulse response of a Maxwell earth, Rev. geophys. space Phys., 12, 649.
- Post, R. & Griggs, D., 1973. The earth's mantle: Evidence of non-Newtonian flow, Science, 181, 1242.
- Rundle, J. & Jackson, D., 1976a. A viscoelastic relaxation model for post-seismic deformation from the San Francisco earthquake of 1906, in preparation.
- Rundle, J. & Jackson, D., 1976b. A viscoelastic model of the San Andreas fault zone applied to the San Francisco earthquake of 1906, Geophys. J. R. astr. Soc., in preparation.
- Rybicki, K., 1971. The elastic residual field of a very long strike-slip fault in the presence of a discontinuity, Bull. seism. Soc. Am., 61, 79.
- Savage, J. & Burford, R., 1973. Geodetic determination of relative plate motion in central California, J. geophys. Res., 78, 832.
- Stocker, R. & Ashby, M., 1973. On the rheology of the upper mantle, Rev. geophys. space Phys., 11, 392.
- Steketee, J., 1958. On Volterra's dislocations in a semi-infinite elastic medium, Canadian J. Phys., 36, 192.
- Thatcher, W., 1974. Strain release mechanism of the 1906 San Francisco earthquake, Science, 184, 1283.

- Thatcher, W., 1975a. Strain accumulation and release mechanism of the 1906 San Francisco earthquake, J. geophys. Res., 80, 4862.
- Thatcher, W., 1975b. Strain accumulation on the northern San Andreas fault zone since 1906, J. geophys. Res., 80, 4873.
- Whittaker, E. & Watson, G., 1927. A Course of Modern Analysis, 4th ed., Cambridge University Press.

Table 1. Comparison of the coseismic elastic and postseismic viscoelastic angle changes for two different ruptures, each in an elastic layer overlying a viscoelastic half-space (see figure 10). For case I, the layer thickness is 20 km, the fault length is 400 km, the displacement dislocation across the fault face is 4 m and the fault has fractured the entire thickness of the layer. For case II, the layer thickness is 5 km, the fault length is 400 km, the displacement dislocation across the fault face is 4 m and the fracture extends from the surface to 3 km depth.

CASE I			CASE II	
Angle #	Coseismic (sec)	Postseismic viscoelastic change (t = 2 τ) (sec)	Coseismic (sec)	Postseismic viscoelastic change (t = 2 τ) (sec)
1	-6.16	-1.83	-3.47	-1.10
2	-13.45	-.98	-9.84	-1.12
3	9.59	2.60	6.40	1.44
4	3.56	-2.03	5.58	-1.97
5	3.87	-1.71	4.50	-1.37
6	-7.43	-3.75	-10.09	3.35
7	-.33	-.04	-.01	-.02
8	.11	-.13	.67	-.19
9	-.07	.18	-.66	.22
10	-12.32	4.60	-.47	10.55
11	16.09	-5.85	57.86	-13.25
12	-3.77	1.24	-10.86	2.70

Table 2. See figure 11. In column 2 are the horizontal surface displacements calculated from the approximate Green's function. Column 3 is the displacements computed with the approximate Greens' function minus the displacements computed by a numerical integration of the exact Green's function.

Source Depth	Approximate Displacements	Displacement Difference	Error
(km)	(cm)	(cm)	(%)
10	87.15	12.36	14.18
9	91.47	11.99	13.11
8	100.52	9.13	9.08
7	114.20	5.60	4.90
6	132.20	.60	.45
5	153.52	-3.49	-2.27
4	176.28	-7.37	-4.18
3	197.35	-11.01	-5.58
2	212.66	-15.01	-7.06
1	<u>217.80</u>	<u>-19.09</u>	<u>-8.77</u>
Totals	1483.15	-16.29	-1.1

Table 3. See figure 12. Columns 2 - 4 are the same as in table 2.

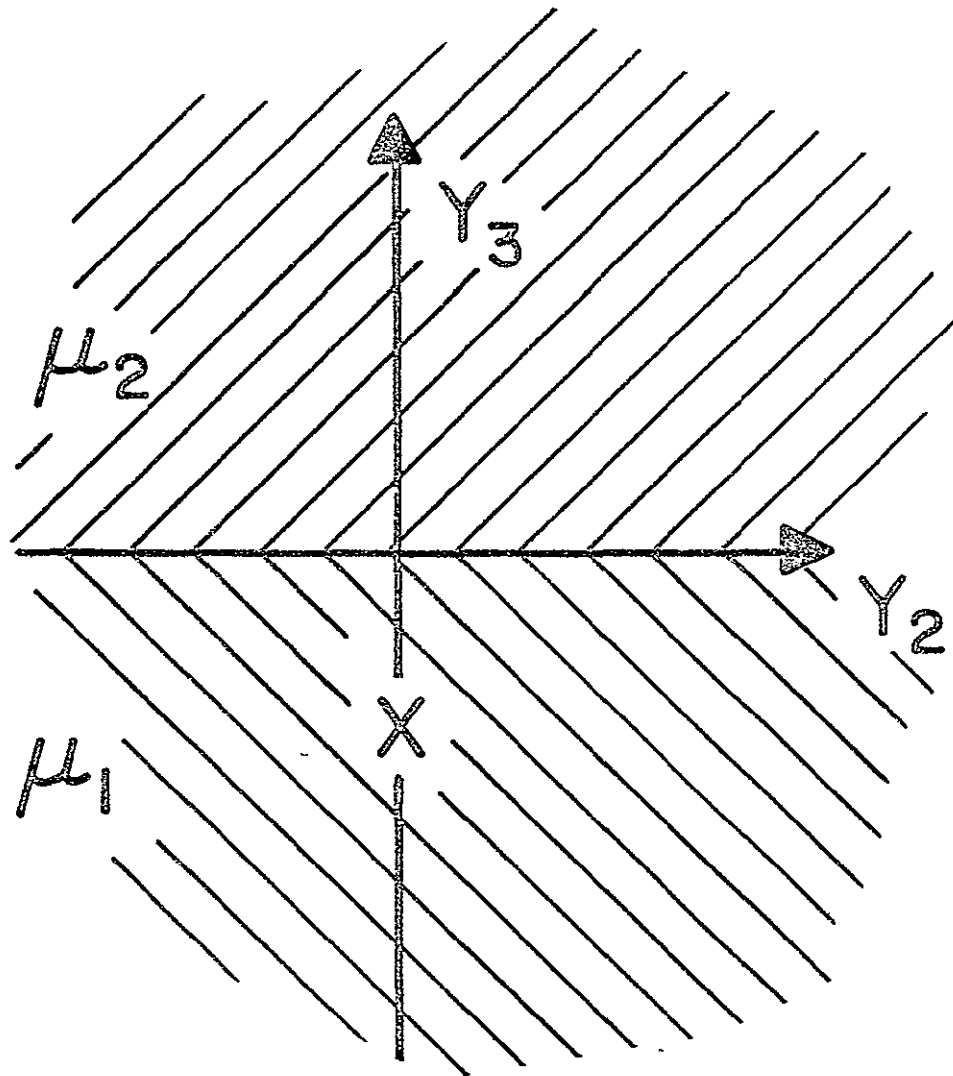
Layer Thickness	Approximate Displacement	Displacement Difference	Error
<u>(km)</u>	<u>(cm)</u>	<u>(cm)</u>	<u>(%)</u>
10	87.15	12.47	14.31
15	52.04	-.75	-1.44
20	48.00	-2.37	-4.94
25	47.14	-1.72	-3.65
30	46.85	-1.18	-2.52

Figure Captions

- Figure 1. Coordinate system used in finding the displacements due to a line dipole of force in the \bar{y}_1 direction.
- Figure 2. Coordinate system used to find the displacements due to a line dipole of force in the y_1 direction for a medium consisting of an elastic layer overlying an elastic half-space.
- Figure 3. Coordinate system for the integration of the Green's function for a strike slip point source. The relative displacement across the rectangular fault surface shown is indicated by the two parallel half-arrows. After Chinnery, M., Bull. seism. Soc. Am., 53, p. 9,, 1963, copyrighted by the Seismological Society of America.
- Figure 4. A Maxwell element.
- Figures 5-7. Surface displacements parallel to a rectangular fault in an elastic layer over a viscoelastic half-space calculated using the approximate Green's function. The displacements were calculated along the horizontal profile shown at the top of each figure where the double arrows lie along the fault trace. The layer thickness is 20 km and the fault fractured the entire thickness of the later. The relative displacement along the fault is 4 m.
- Figures 8-9. Surface displacements perpendicular to a rectangular fault in an elastic layer over a viscoelastic half-space

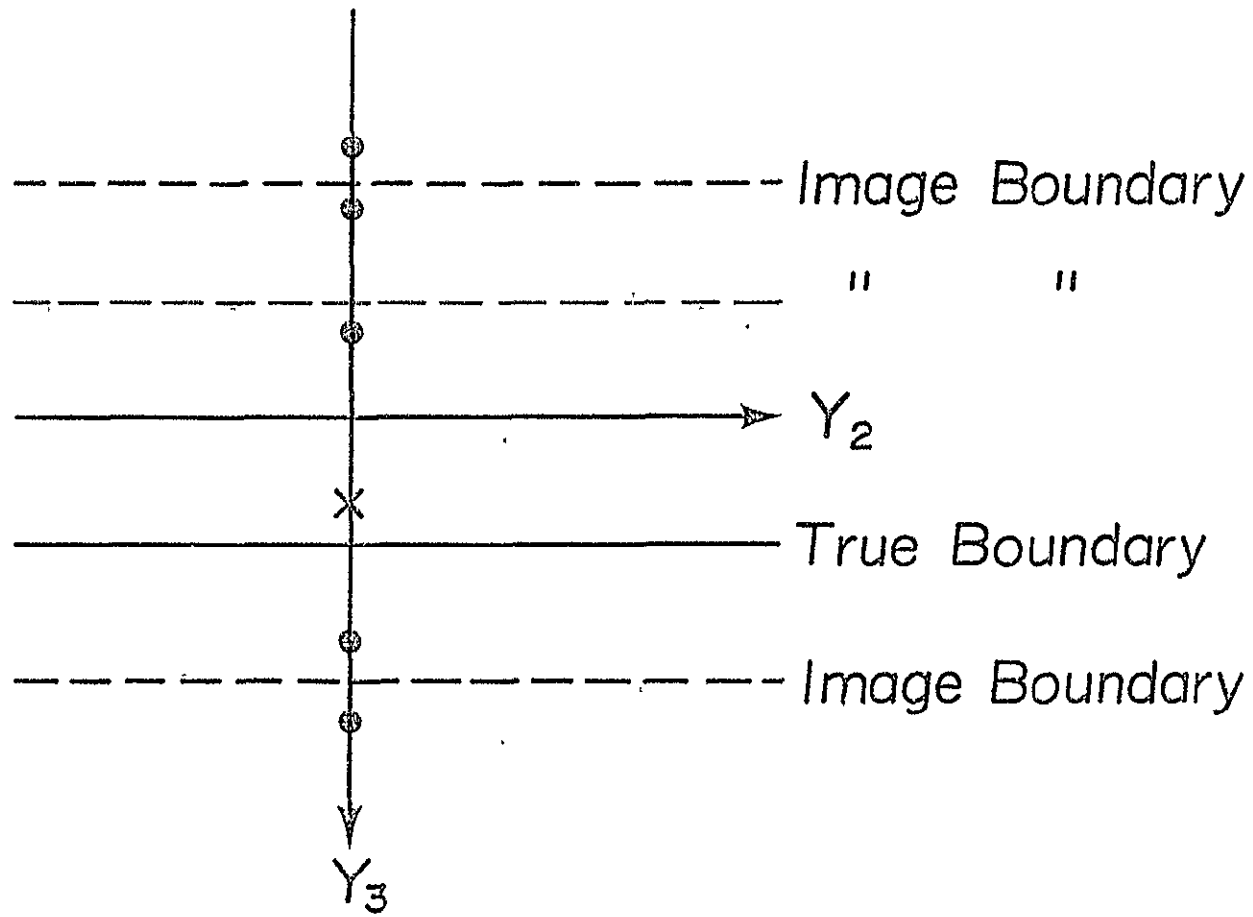
All parameters are the same as for figures 5 - 7.

- Figure 10. Location of some illustrative model survey triangles relative to a rectangular fault in an elastic layer over a viscoelastic half-space (see Table 1). The fault is indicated by the double arrows, and the insert is a blow-up of the cross-hatched region. All angle changes were computed using the approximate Green's function.
- Figure 11. Plot of the differences in the predicted horizontal surface displacements due to using the approximate Green's function in place of a numerical integration of the exact Green's function for a point source in an elastic layer over an elastic half-space. H is fixed at 10 km and the rigidity of the layer is one-tenth the rigidity of the half-space. The point of observation is at a radial epicentral distance of 10 km. See Table 2.
- Figure 12. Plot of the differences in the predicted horizontal surface displacements due to using the approximate Green's function in place of a numerical integration of the exact Green's function for a point source in an elastic layer over an elastic half-space. The rigidity of the layer is one-tenth the rigidity of the half-space and the point of observation is at a radial epicentral distance of 10 km. The source depth is fixed at 10 km. See Table 3.



X Source point at X_3

PRECEDING PAGE BLANK NOT FILMED



- \times Source Point at X_3
- \bullet Image Source Points

